Int. J. Electrochem. Sci., 11 **(2016)** 4560 – 4585, doi: 10.20964/2016.06.44

International Journal of
ELECTROCHEMICAL
SCIENCE
www.electrochemsci.org

Modeling the Effect of Piperazine on Carbon Steel Corrosion Rate in Carbonated Activated MDEA Solutions

Lubna Ghalib[1,2], *Brahim Si Ali*[1,*], *Shaukat Mazari*[1] ,*Wan Mohd Ashri*[1], *Idris Mohamed Saeed*[1]

[1]Department of Chemical Engineering, University of Malaya, 50603 Kuala Lumpur, Malaysia
[2]Department of Material Engineering, University of Al-Mustansiriyah, 10052 Baghdad, Iraq
[*]E-mail: brahim@um.edu.my

Received: 24 December 2015 / *Accepted:* 3 April 2016 / *Published:* 4 May 2016

A comprehensive model is developed for simulating the rate of corrosion of carbon steel in carbonated aqueous activated MDEA (Methyl-di-ethanolamine) solutions. The model includes VLE (Vapor Liquid Equilibrium) and the electrochemical behavior of amine systems. The VLE model is used to predict the speciation of aqueous carbonated MDEA-PZ solutions and their concentrations, activity coefficients, and transport properties. The electrochemical model simulates partial oxidation and reduction processes on the surface of carbon steel. The model was capable to predict the effect of PZ (piperazine) concentration on the carbon steel corrosion rate, for carbonated solutions of MDEA/PZ blends. The model is executed in a Matlab program that simulates the effect of process operating conditions such as solution temperature, CO_2 loading, solution pH, total amine concentration, and PZ concentration on carbon steel corrosion rates. Results of speciation and corrosion models are in good agreement with the experimental findings.

Keywords: CO_2 capture, CO_2 corrosion, Methyl-di-ethanolamine, Piperazine, Carbon steel, Polarization curve.

1. INTRODUCTION

Amine-based-CO_2 absorption process has gained interest as an immediate technological solution for CO_2 capture from flue gas streams of coal-fired power plants. The amine scrubbing technology is well established for the sweetening of utility gas streams. On the other hand, yet it suffers from design and operational (solvent volatility, degradation, and corrosivity) problems for post-combustion CO_2 capture [1, 2]. Aspect of corrosion is one of the main challenges in post-combustion CCS (carbon capture and storage), which ultimately affects solvent performance efficiency, plant operation and safety. Since corrosion cannot be avoided, it has to be understood in order to select the

material of construction, inhibitors and process parameters. Corrosiveness of amine solutions during CO_2 absorption depends on various parameters such as the type and concentration of amine, CO_2 loading, temperature, and the presence and types of degradation products [3].

A preferred amine system in recent years for the amine scrubbing process is activated methyl-di-ethanolamine. The activated MDEA system is considered a physical absorption system at high CO_2 partial pressure and chemical absorption at low CO_2 partial pressure [4]. Piperazine using as an activator in MDEA is one of the favored subjects of investigation in the recent years [5-7]. Piperazine is an effective promoter in CO_2 absorption using amine scrubbing process [6, 8, 9].

Corrosion studies of some of the blends of PZ on carbon steel has been conducted recently [10, 11].Corrosion in tin presence of activated MDEA solutions was studied by Zhao et al. [10], showing the same detrimental impact of CO_2 loading and temperature as already observed in MEA (monoethanolamine) or other amine systems. Corrosion product layers of carbon steel were investigated in CO_2-saturated MDEA solutions under 4.5 MPa CO_2 at 100 °C by Guo and Tomoe [12]. Results of Zheng [13] show that the formation of $FeCO_3$ layer on the surface of carbon steel in carbonated aqueous PZ solutions at high temperature was dense, stable and protective that results a sharp decrease in carbon steel corrosion rate. However, knowledge of the corrosion behavior on carbon steel in activated amine solutions is still not well understood. Choi et al. [14] developed a predictive model for corrosion of carbon steel in CO_2-loaded aqueous methyl-di-ethanolamine systems, based on modeling of thermodynamic equilibria and electrochemical reactions. This model is applicable to uniform corrosion when no protective films are present.

Objective of this work is to develop a mechanistic corrosion rate model of carbon steel in aqueous carbonated solutions of activated methyl-di-ethanolamine under absorber operating conditions. Effect of activator concentration at various temperatures on the corrosion behavior of carbon steel in carbonated solution is investigated.

2. ELECTROCHEMICAL SETUP

2.1 Materials

The specimens were made of carbon steel with a chemical composition of C, 0.20; Mn, 0.51; P, 0.013; S, 0.039; Si, 0.17 and balanced Fe. The specimens were manufactured and supplied by the corrosion meter company (Radiometer France). They were shaped cylindrical, and inserted tight into Teflon. The cylinder base disc was with surface area of 0.196 cm^2. The specimen was threaded into the rotating electrode, which was connected to the radiometer FCTV101. Carbon steel was chosen as it is generally used in the absorber, lean amine cooler tubes, reflux drum, and regenerator shell. The specimens were ground with 600 grit silicon carbide paper.

Aqueous solutions of activated MDEA were prepared using double distilled water from 99% MDEA reagent, PZ flakes (99% purity), which were purchased from Acros Organics and Merck Millipore respectively. The partial pressure of CO_2 in the flowing gas stream was varied from 1 kPa to 100 kPa by adjusting the flow rates of CO_2 and N_2 of known composition in the reaction gas. The total

pressure of the reactor was monitored using a pressure transducer, temperature ranged from 40 to 80 °C, and total amine concentration was kept 2.0 M. In the mixtures of MDEA/PZ, the piperazine concentration was varied from 0.01 M to 0.1 M.

2.2. Potentiodynamic polarization measurements

The corrosion tests were carried out in a 250 ml cell under atmospheric pressure. The setup consisted of a jacketed cell equipped with the following accessories a: (1) three - electrode corrosion cells, platinum wire counter electrodes (auxiliary electrode), a calomel reference electrode, and a working electrode; (2) hot plate equipment with temperature controller; (3) gas (nitrogen and carbon dioxide) supplied on the top of the solution to maintain the CO_2 loading in the solution; (4) Potentiostat /Galvanostat and a radiometer FCTV101;(5) pH meter. The schematic of experimental setup is shown in Figure 1.

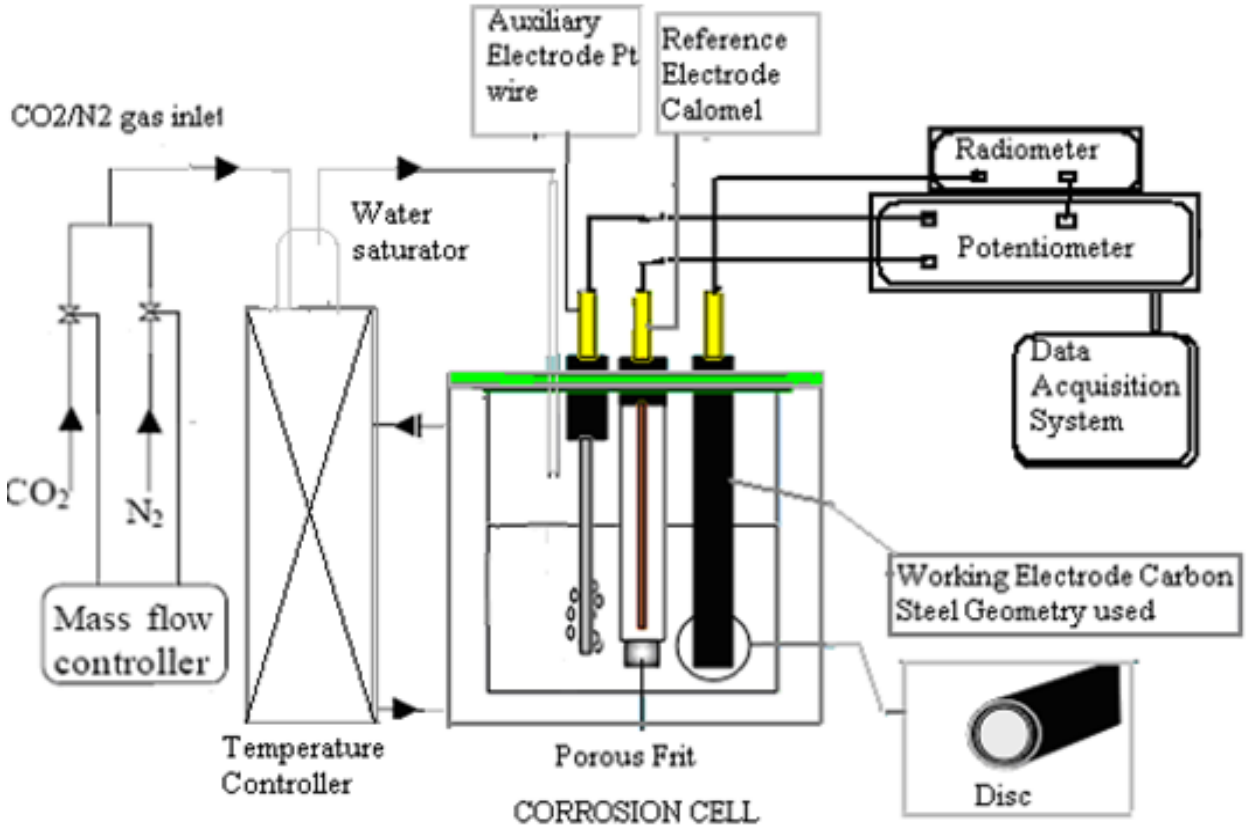

Figure 1. Schematic of the electrochemical experimental setup for corrosion experiment [15].

During each run, a gas mixture of CO_2 and N_2 was bubbled through the cell until gas-liquid equilibrium was attained when a constant pH of solution was observed. Then, potentio-dynamic technique was used to run the corrosion tests. In this procedure, before each polarization experiment the carbon steel working electrode surface (specimen) was polished with 600 grit silicon carbide

papers. Then mounted on the specimen holder (rotating working electrode), and immersed into the carbonated activated MDEA solution. The working electrode was subjected to a constant rotation speed of 600 rpm through a radiometer speed control unit.

Potential scanning was effected using a radiometer potentiostat /galvanostat connected to a PC coupled with a control and data acquisition system. The potentio-dynamic sweep technique was used to investigate the corrosion mechanism. The sweeps were conducted with a scan rate of 1.8 mV/sec.

The corrosion potential (E_{corr}) and corrosion current density (i_{corr}) were calculated from the intersection of anodic and cathodic Tafel slopes of the polarization curves using EC-Lab software V10.12, 2011. The corrosion rate (CR) was calculated using the following equation:

$$CR = \frac{3.30 \times 10^{-3} \times i_{corr}\, MW}{\rho}$$

Where CR is the rate of corrosion (mm/yr), i_{corr} is corrosion current density (μA/cm^2), MW is the molar weight of the specimen (g/mol), and ρ is the density of specimen (g/m^3).

3. SPECIATION MODEL

3.1 Vapor-liquid equilibrium model

In an open system, due to unlimited supply of gas, there is a constant partial pressure of carbon dioxide gas species on the surface of the amine solution in amine scrubbing process. Vapor-liquid equilibrium of carbon dioxide reaction is described as:

R1: CO_2 phase change: $CO_2(g) \overset{K_1}{\leftrightarrow} CO_2(aq)$

When carbon dioxide is dissolved in aqueous solution containing PZ and MDEA, aqueous carbon dioxide undergoes a sequence of chemical reactions as follows [16, 17]. Carbonic acid (H_2CO_3) is not included here as it is in much lower concentration compared to other carbonic species (HCO_3^- and CO_3^{2-}). In the follow-up electrochemical work it was confirmed that H_2CO_3 does not contribute much to the overall corrosion process and could be omitted from the analysis [14].

R2: Dissociation of water: $2H_2O \overset{K_2}{\leftrightarrow} OH^- + H_3O^+$

R3: Dissociation of CO_2: $CO_2 + 2H_2O \overset{K_3}{\leftrightarrow} HCO_3^- + H_3O^+$

R4: Dissociation of bicarbonate ions: $HCO_3^- + H_2O \overset{K_4}{\leftrightarrow} CO_3^{2-} + H_3O^+$

R5: Dissociation of protonated piperazine: $PZH^+ + H_2O \overset{K_5}{\leftrightarrow} PZ + H_3O^+$

R6: Formation of piperazine carbamate: $PZ + CO_2 + H_2O \overset{K_6}{\leftrightarrow} PZCOO^- + H_3O^+$

R7:Dissociation of zwitterion (protonated carbamate): $H^+PZCOO^- + H_2O \overset{K_7}{\leftrightarrow} PZCOO^- + H_3O^+$

R8: Dissociation of piperazine carbamate: $PZCOO^- + CO_2 + H_2O \overset{K_8}{\leftrightarrow} PZ(COO^-)_2 + H_3O^+$

R9: Dissociation of protonated methyl-di-ethanolamine: $MDEAH^+ + H_2O \overset{K_9}{\leftrightarrow} MDEA + H_3O^+$

Where: K is the equilibrium constant of reversible reaction at equilibrium, which were obtained from literature and are given in Table 1 on a mole fraction basis. The K_i of the above reactions is expressed in terms of activity coefficient (γ_i) and mole fraction chemical species (x_i), as given in equation 1 through 8:

$$K_1 = \frac{(\gamma_{H_3O^+} x_{H_3O^+})(\gamma_{OH^-} x_{OH^-})}{(\gamma_{H_2O} x_{H_2O})^2} \quad (1)$$

$$K_2 = \frac{(\gamma_{HCO_3^-} x_{HCO_3^-})(\gamma_{H_3O^+} x_{H_3O^+})}{(\gamma_{CO_2} x_{CO_2})(\gamma_{H_2O} x_{H_2O})^2} \quad (2)$$

$$K_3 = \frac{(\gamma_{CO_3^{2-}} x_{CO_3^{2-}})(\gamma_{H_3O^+} x_{H_3O^+})}{(\gamma_{HCO_3^-} x_{HCO_3^-})(\gamma_{H_2O} x_{H_2O})} \quad (3)$$

$$K_4 = \frac{(\gamma_{PZ} x_{PZ})(\gamma_{H_3O^+} x_{H_3O^+})}{(\gamma_{PZH^+} x_{PZH^+})(\gamma_{H_2O} x_{H_2O})} \quad (4)$$

$$K_5 = \frac{(\gamma_{PZCOO^-} x_{PZCOO^-})(\gamma_{H_3O^+} x_{H_3O^+})}{(\gamma_{PZ} x_{PZ})(\gamma_{CO_2} x_{CO_2})(\gamma_{H_2O} x_{H_2O})} \quad (5)$$

$$K_6 = \frac{(\gamma_{PZCOO^-} x_{PZCOO^-})(\gamma_{H_3O^+} x_{H_3O^+})}{(\gamma_{H^+PZCOO^-} x_{H^+PZCOO^-})(\gamma_{H_2O} x_{H_2O})} \quad (6)$$

$$K_7 = \frac{(\gamma_{PZ(COO^-)_2} x_{PZ(COO^-)_2})(\gamma_{H_3O^+} x_{H_3O^+})}{(\gamma_{PZCOO^-} x_{PZCOO^-})(\gamma_{CO_2} x_{CO_2})(\gamma_{H_2O} x_{H_2O})} \quad (7)$$

$$K_8 = \frac{(\gamma_{MDEA} x_{MDEA})(\gamma_{H_3O^+} x_{H_3O^+})}{(\gamma_{MDEAH^+} x_{MDEAH^+})(\gamma_{H_2O} x_{H_2O})} \quad (8)$$

In addition, Henry's law can express the physical solubility of CO_2 absorption in amine solution:

$$P_{CO_2} = H_{CO_2}[CO_2] \quad (9)$$

Where: P_{CO_2} is the partial pressure of CO_2, measured during the experiment; H_{CO_2} is the Henry's law constant for CO_2, which is a function of temperature as shown in Table 1. To quantify bulk concentration of all chemical species, the additional equations for each solution are listed as in equation 10 through 14:

Electro neutrality balance:

$$MDEAH^+ + PZH^+ + H_3O^+ = HCO_3^- + OH^- + 2\,CO_3^{2-} + PZCOO^- + 2PZ(COO^-)_2 \quad (10)$$

Mole balance for PZ:

$$PZ + PZH^+ + PZCOO^- + H^+PZCOO^- + PZ(COO^-)_2 = PZ_{Total} \quad (11)$$

Mole balance for MDEA:

$$MDEA + MDEAH^+ = MDEA_{Total} \quad (12)$$

Total mole fraction:

$$\sum_{i=1}^{i=N} x_i = 1.0 \quad (13)$$

Mole balance for CO_2:

$$CO_2 + HCO_3^- + CO_3^{2-} + PZCOO^- + H^+PZCOO^- + PZ(COO^-)_2 = CO_{2\,Total} \quad (14)$$

3.2 Calculation of fugacity coefficients

Under the established phase equilibria, the fugacity of each constituent in the liquid and vapor phase are identical. Under equilibrium conditions, CO_2 molecules distribution takes place between liquid and vapor phases as per equation (15). However, water, PZ, and MDEA distribute themselves according to activity coefficient approach as in equation (16) [18].

$$\emptyset^v_{co_2} y_{co_2} P = \gamma^*_{co_2} x_{co_2} H^\infty_{co_2} \exp\left(\frac{v^\infty_{co_2}(P - P^s_W)}{RT}\right) \quad (15)$$

$$\emptyset_i^v y_i P = \gamma_i x_i P_i^\circ \emptyset_i^\circ \exp\left(\frac{v_i\left(P-P_i^\circ\right)}{RT}\right) \quad (16)$$

Where y_i and x_i are concentration of species in vapor and liquid phases, respectively, $v_{co_2}^{\infty}$ partial molar volume of CO_2 at infinite dilution was calculated by using the Brlvi-O'Connell method. P^o is the vapor pressure and $\emptyset_i^v$ vapor phase fugacity coefficient. The Soave–Redlich-Kwong (SRK) equation of state have been made in use to calculate the vapor phase fugacity coefficients for equations (15) and (16) [19] and the liquid phase activity coefficients are calculated using the e-NRTL (electrolyte – nonrandom two liquid) model.

Table 1. Temperature dependence of equilibrium constants and Henry's constant

Component	C_1	C_2	C_3	C_4	T(K)	Reference
Equilibrium constant: $\ln K_i = C_1 + \frac{C_2}{T} + C_3 \ln T + C_4 T$						
K_1	132.9	-13446	-22.48	0.0	273-498	[20]
K_2	231.4	-12092	-36.78	0.0	273-498	[20]
K_3	216.0	-12432	-35.48	0.0	273-498	[20]
K_4	-9.6416	-5008.4	0.0	0.0	270-350	[21]
K_5	466.497	1614.5	-97.540	0.2471	273-343	[22]
K_6	6.822	-6066.9	-2.290	0.0036	273-343	[22]
K_7	-11.563	1769.4	-1.467	0.0024	373-343	[22]
K_8	-83.49	-819.7	10.9756	0.0	278-368	[7]
Henry's constant: $\ln H_{co_2} = C_1 + \frac{C_2}{T} + C_3 \ln T + C_4 T$						
H_{CO2}	170.71	-8477.7	-21.95	0.005781	273-373	[17]

3.3 Calculation of activity coefficients

The e-NRTL equation used in the present study to calculate the excess Gibbs energy is presented in equation (17) [17].

$$\frac{G^{ex}}{RT} = \frac{G^{ex,PDH}}{RT} + \frac{G^{ex,Born}}{RT} + \frac{G^{ex,lc}}{RT} \quad (17)$$

$$\frac{G^{ex,PDH}}{RT} = -\sum_k x_k \left(\frac{1000}{M_s}\right)^{\frac{1}{2}} \left(\frac{4A_\phi I_x}{\rho}\right) \ln\left(1+\rho I_x^{\frac{1}{2}}\right) \quad (18)$$

Where Debye–Hückel parameter (A_ϕ) and ionic strength of solvent (I_x), are given by equations (19) and (20), respectively.

$$A_\phi = \frac{1}{3}\left(\frac{2\pi N_A d_s}{1000}\right)^{\frac{1}{2}} \left(\frac{e^2}{DkT}\right)^{\frac{3}{2}} \quad (19)$$

$$I_x = \frac{1}{2}\sum_i x_i Z_i^2 \quad (20)$$

The Born correction term for the excess Gibbs energy is presented by equation (21):

$$\frac{G^{ex,Born}}{RT} = \left(\frac{e^2}{2kT}\right)\left(\frac{1}{D}-\frac{1}{D_W}\right)\left(\sum_i \frac{x_i z_i^2}{r_i}\right) \times 10^{-2} \quad (21)$$

Mass fraction averages were used to calculate the mixed solvent dielectric constants. The dielectric constants for solvent constituents are presented in Table 2. The e-NRTL expression for the short-range interaction is given as in equation (22):

$$\frac{G^{ex,lc}}{RT} = \sum_m X_m \frac{\sum_j X_j G_{jm}\tau_{jm}}{\sum_k X_k G_{km}} + \sum_c X_c \sum_{a'} \left(\frac{X_{a'}}{\sum_{a''} X_{a''}}\right) \frac{\sum_j X_j G_{jc,a'c}\tau_{jc,a'c}}{\sum_k X_k G_{kc,a'c}} + \sum_a X_a \sum_{c'} \left(\frac{X_{c'}}{\sum_{c''} X_{c''}}\right) \left(\frac{\sum_j X_j G_{ja,c'a}\tau_{ja,c'a}}{\sum_k X_k G_{ka,c'a}}\right) \quad (22)$$

Where; j and k are any species, and the quantities of all terms in equation (22) are defined as in equation (23) through (26)

$$G_{jc,a'c} = \exp\left(-\alpha_{jc,a'c}\,\tau_{jc,a'c}\right) \quad (23)$$

$$G_{ja,c'a} = \exp\left(-\alpha_{ja,c'a}\,\tau_{ja,c'a}\right) \quad (24)$$

$$\tau_{cm} = -\frac{\ln G_{cm}}{\alpha_{cm}} \quad (25)$$

$$\tau_{am} = -\frac{\ln G_{am}}{\alpha_{am}} \quad (26)$$

Where; c, a, and m represent cations, anions and molecular species, respectively. $X_j=x_j.C_j$ ($C_j=z_j$ for ions and 1 for molecules); α_{ij} is the non-randomness factor and τ_{ij} is the binary energy interaction parameter. The activity coefficients of all species in the solution are calculated from the partial derivative of the excess Gibbs energy with respect to mole number as per equation (27):

$$ln\,\gamma_i = \frac{1}{RT}\left[\frac{\partial(n_t G^{ex})}{\partial n_i}\right]_{T,P,n_{j\neq i}} \qquad i\,,\ j= m, c, a \quad (27)$$

Table 2. Dielectric constants (D) of MDEA, PZ, and H_2O [16]

Species	a_1	b_1
H_2O	88.36	33030
PZ	36.76	14836
MDEA	24.76	8989

$D = a_1 + \frac{b_1}{T}\left[\frac{1}{T} - \frac{1}{273.15}\right]$, where T in (K)

3.4 Speciation Model parameters

The pure component parameters, such as critical constants, acentric factor, Brelvi–O'Connell parameters, critical compressibility factor used in the Rackett model and the Antoine equation coefficients for the vapor pressure of molecular species were obtained from the literature and are summarized in Tables 3 and 4.

Table 3. Physical properties of pure component for VLE model

Properties	CO_2	H_2O	PZ	MDEA
Tc (K)	304.20	647.30	638.0	677.79
Pc (kPa)	7376.0	22048	6870	3876
Vc (m^3 /kmol)	0.0939	0.0559	0.3100	0.39
Acentric factor (ω)	0.2250	0.3440	0.4138	1.24
Racket Z_{RA}	0.2736	0.2432	0.2000	0.19
Brelvi-O'Connell parameter	0.0939	0.0464	-	-

Both α and τ are adjustable parameters of the electrolyte NRTL expression. For the CO_2–amine system, the non-randomness parameter α was fixed at specific values, i.e. 0.2 for both molecule–molecule ($\alpha_{m,m'}$) and water–ion pair ($\alpha_{w,ca}$ or $\alpha_{ca,w}$) interactions and 0.1 for both amine–ion pair and CO_2–ion pair interactions. The binary energy interaction parameter τ are consistent with those from the work of Austgen et al. [17] and Posey [20]. These binary parameters are categorized into three groups; molecule–molecule pair, molecule–ion pair (or ion pair–molecule) and ion pair–ion pair interactions. Because of their insignificance, the ion pair–ion pair parameters were set to a default value of zero [17]. Water–ion pair and ion pair–water parameters were fixed at default values of 8.0 and - 4.0, respectively. Amine–ion pair and ion pair– amine binary parameters and all CO_2–ion pair and ion pair–CO_2 binary parameters were fixed at values of 15.0 and - 8.0, respectively.

Table 4. Antoine equation coefficients of molecular species

Components	CO_2	H_2O	PZ	MDEA
A	72.82912	72.55	70.503	29.137
B	-3403.28	-7206.7	-791.45	-7588.5
C	0.0	0.0	0.0	0
D	9.49E-03	0.0	0.0	0
E	-8.56034	-7.1385	-6.6461	0
F	2.91E-16	4.05E-06	5.21E18	0
G	6	2	6	0

3.5 Mathematical framework for speciation

A Matlab program based on the above equations was developed for predicting species concentration in the aqueous CO_2-PZ-MDEA systems. Concentrations of all species were unknown and defined as independent variables except the concentrations of CO_2, which were calculated by the equation (9). Consequently, twelve equations (1) – (8), (10) – (13) with twelve unknowns were solved by reducing them to a single seventh order polynomial in terms of hydronium ion concentration

$[H_3O^+]$, initial amine concentration and equilibrium constants. The value of $[H_3O^+]$ is associated with the pH of the solution at equilibrium. There is more than one possible solution for each CO_2 partial pressure. However, only one value of $[H_3O^+]$ is valid and should lie between 10^{-6} mol/l and 10^{-12} mol/L. This corresponds to values of pH of 6 and 12 respectively. The concentrations of other species then can be calculated. Equations were solved simultaneously using the iteration process of twelve non-linear equations. The obtained outputs are species concentration and activity coefficients for the chemical species.

4. ELECTROCHEMICAL CORROSION MODEL

4.1 Electrochemical reactions on the metal surface

The electrochemical corrosion model describes the electrochemical behavior taking place on steel surface that is exposed to aqueous carbonated solutions of PZ- MDEA. It is assumed that the oxidation reaction is the conversion of Fe to Fe^{2+} while the reduction reactions involve five reactions due to the presence of five reducing agents including H_3O^+, HCO_3^-, H_2O, PZH^+ and $MDEAH^+$. The summary of the assumed reactions taking place on surface of the carbon steel are provided by the following reactions:

Oxidation of iron: $Fe \leftrightarrow Fe^{2+} + 2e^-$

Reduction of hydronium ion: $2H_3O^+ + 2e^- \leftrightarrow 2H_2O + H_2$

Reduction of bicarbonate ion: $2HCO_3^- + 2e^- \leftrightarrow 2CO_3^{2-} + H_2$

Reduction of water: $2H_2O + 2e^- \leftrightarrow 2OH^- + H_2$

Reduction of PZH^+ ion: $2PZH^+ + 2e^- \leftrightarrow 2PZ + H_2$

Reduction of $MDEAH^+$ ion: $2MDEAH^+ + 2e^- \leftrightarrow 2MDEA + H_2$

4.2 Mathematical model for the electrochemical corrosion process

The dissolution of iron was said to be under charge transfer control because of the unlimited supply of Fe. The relationship between current density and potential was defined as in equation (28) and (29):

$$i_{Fe/Fe^{+2}} = i_{o,Fe/Fe^{+2}} \times 10^{\left(\frac{E-E_{rev}}{\beta_a}\right)} \quad (28)$$

$$\beta_a = \frac{2.303\ RT}{n\ \alpha_a F} \quad (29)$$

For the reduction, potential reactants participating in corrosion process are reduction reaction of H_3O^+, reduction reaction of HCO_3^-, reduction reaction of H_2O, reduction reaction of PZH^+ and reduction reaction of $MDEAH^+$, in which H_3O^+, HCO_3^-, H_2O, PZH^+, and $MDEAH^+$ serve as oxidizing agents. The reduction reactions were assumed to be under mixed potential. For the system of (*k*) reduction reactions, the general rate equation of the cathodic part is as in equation (30):

$$i_k = i_{o(k)} \times \left\{\frac{[k]_s}{[k]_b} \times \exp\left(-\frac{n\ \alpha_c F}{RT}(E - E_{rev})\right)\right\} \quad (30)$$

Where: i_k is the current density of a reduction reaction (A/m^2). i_o is the equilibrium exchange current density of a reaction (A/m^2). $[k]_s$ is the surface concentration of oxidizing agent species (mol/l). $[k]_b$ is the bulk concentration of oxidizing agent species (mol/l). α_c ; is the cathodic symmetry factor. n; is the number of electrons transferred in the reduction reaction. F; is the Faraday's constant(C/mol) and E; is the potential (V.vs SCE). Equation (30) takes into account the effect of resistance to charge transfer and mass transfer. The surface concentration of oxidizing agents can be determined from the mass-transfer equation:

$$i_k = k_m F \{[k]_b - [k]_s\} \quad (31)$$

Where k_m; is the reduction reaction mass-transfer coefficient (m/s). Substitution of equation (30) into (31) and solving for $[k]_s$ yields the final current density vs voltage equation for reduction reactions:

$$\frac{1}{i_k} = \frac{1}{i_{act(k)}} + \frac{1}{i_{lim(k)}} \quad (32)$$

Where $i^d_{lim(k)}$ is the diffusion limiting current density in A/m^2 and $i_{act(k)}$ is the activation current density in absence of resistance to mass transfer, which is given by equation (33):

$$i_{act(k)} = i_{o(k)} \times 10^{\left(-\frac{(E-E_{rev})}{\beta_c}\right)} \quad (33)$$

Where; $i_{o(k)}$; is the exchange current density in A/m^2 and β_c; is the cathodic Tafel slope in V/dec. The temperature dependence of the cathodic Tafel slope is given as in equation (34):

$$\beta_c = \frac{2.303\ RT}{n\ \alpha_c F} \quad (34)$$

The reversible potential E_{rev} (V vs SCE) for species in the solution, which is calculated from the Nernst equation; equation (35):

$$E_{rev} = E^o_T + \frac{RT}{nF} \ln\left(\frac{a_{prod.}}{a_{react.}}\right) \quad (35)$$

Where: E_T^o is the standard electrode potential (V vs SCE) at any given temperature, R; is the universal gas constant (J/mol.K), T; is the absolute temperature (K), n; is the number of electrons taking part in the reaction. $a_{prod.}$ and $a_{react.}$ are the activities of products and reactants, respectively, F; is the Faraday's constant (C/mol). The E_T^o; was determined using equation (36):

$$\Delta G^o_T = -n_i F E^o_T \quad (36)$$

Where ΔG^o_T is the Gibbs free energy of formation of any compound at any given temperature, which can be calculated using equation (37):

$$\Delta G^o_T = T\left[\frac{\Delta G^o_r}{298.15} + \Delta H^o_r\left(\frac{1}{T} - \frac{1}{298.15}\right)\right] \quad (37)$$

Where ΔG^o_r and ΔH^o_r are standard excess Gibbs energy (kJ/mol) of reaction at 298.5 K and standard enthalpy of reaction (kJ/mol) at 298.15 respectively and T is the system temperature (K). The values of ΔG^o_r and ΔH^o_r are given in Table 5.

While the temperature dependence of the exchange current density is given by equation (38):

$$i_o = i_{o,ref}\left(\frac{C_{ox}}{C_{ox,ref}}\right)^n \exp\left(-\frac{E_a}{R}\left(\frac{1}{T} - \frac{1}{T_{ref}}\right)\right) \quad (38)$$

Where E_a: is the activation energy in kJ/mol and i_o^{ref} is the reference exchange current density measured at the reference temperature, T_{ref} and reference concentration of oxidizing agent, C_{ox} is the concentration of oxidizing agent, and *n* is the order of reaction.

Table 5. Gibbs free energy and enthalpy of reactions

Reaction	ΔG_r^o (kJ/mol)	ΔH_r^o (kJ/mol)	Source
Oxidation of Fe	84.9	87.9	[23]
Reduction of H_3O^+	0.0	0.0	[23]
Reduction of HCO_3^-	118	29.8	[23]
Reduction of H_2O	159.8	111.6	[23]
Reduction of $MDEAH^+$	98.46	73.8574	[24]
Reduction of PZH^+	111.09	85.78	[25]

The values were extracted from open literature for the reactions [14, 26]. While the protonated piperazine reduction reaction, the exchange current density was assumed to be similar to that of the exchange current density of protonated MDEA. The diffusion-limiting component of the total current density is as given in equation (39):

$$i_{lim(k)} = nFk_m[k]_b \quad (39)$$

k_m is calculated from rotating cylinder correlation of Eisenberg, et al. [27]

$$Sh = \frac{k_m d}{D} = 0.0791 \times Re^{0.7} \times Sc^{0.33} \quad (40)$$

Where; Sh is Sherwood number, D is diffusion coefficient of species (m^2/s), Re; is Reynold number, Sc; is Schmitt number and d; is diameter of rotating disc (m). The temperature effect on diffusion coefficient was found from the Stokes-Einstein equation; equation (41):

$$D = D_{ref} \times \frac{T}{T_{ref}} \times \frac{\mu_{ref}}{\mu} \quad (41)$$

Where; D_{ref} is the diffusion coefficient of species at a reference temperature (T_{ref}), μ_{ref}; is the dynamic viscosity of aqueous MDEA-PZ solution at a reference temperature (T_{ref}) and μ; is the viscosity of aqueous MDEA-PZ solution at temperature (T). The diffusion coefficients of ionic species are provided in Table 6 and the values of μ (Ns/m^2) can be determined from equation(42) [28]:

$$\mu_{mix} = \frac{w_1}{w_1+w_2}\mu_{1,\alpha} + \frac{w_2}{w_1+w_2}\mu_{2,\alpha} \quad (42)$$

Where μ_{mix} is the viscosity of carbonated aqueous MDEA-PZ solution, μ_1 and μ_2 are the viscosities of aqueous MDEA and aqueous PZ at CO_2 loading α and w_i the mass fraction of MDEA and PZ. The viscosity of single alkanolamine in (Ns/m^2) can be determined from equation (43) [28]:

$$\mu_i = \mu_{H_2O}\, exp\left[\frac{[(a_i w_1 + b_i)T + (c_i w_1 + d_i)][\alpha(e_i w_1 + f_i T + g_i) + 1] w_1}{T^2}\right] \quad (43)$$

Where μ_i; is the viscosity of aqueous single solvent (kg/m.s) at any given temperature T, μ_{H_2O} is the viscosity of water (kg/m.s) at any given temperature T, T is the given temperature (K), α is the CO_2 loading (mol CO_2 /mol amine), w_1 is the mass percent of MDEA or PZ, a, b, c, d, e, f, and g are constants and are given in Table 7. The value of μ_{H_2O} can be determined as a function of the temperature as shown in equation (44).

$$\mu_{H_2O} = \mu_{H_2O,ref} \times 10^{\left(\frac{1.3277\,(20-T) - 0.001053\,(T-20)^2}{T-105}\right)} \quad (44)$$

Where $\mu_{H_2O,20\,^oC}$ is the viscosity of water at 20 °C (0.001002 NS/m^2) and T is the temperature (°C).

Table 6. Diffusion coefficients of various species in water at 298.15 K

Species	Diffusion coefficient (m^2/s)	Sources
H_2O	2.26E-09	[29]
HCO_3^-	1.11E-09	[30]
H_3O^+	9.31E-09	[30]
$MDEAH^+$	2.35E-10	[31]
PZH^+	5.66E-10	[32]

Table 7. Parameters for MDEA and PZ viscosity equation

Constant	a	b	c	d	e	f	g	Sources
MDEA	-0.1944	0.4315	80.684	2889.1	0.0106	0	-0.2141	[28]
PZ	0.1156	8.444	-9.074	3.224	0.7412	0.0225	-9.074	[33]

4.3 Execution of the corrosion model

The present electrochemical model was executed in Matlab 2013a for simulating the polarization curve of carbon steel in the aqueous MDEA-PZ-CO_2 system. To execute the numerical simulation, solution temperature, amine concentration, CO_2 partial pressure, rotating speed, and electrode diameter were used as inputs. Once all parameters were determined, the model predicted the polarization curve with the individual and total cathodic curves. The intersection of the total cathodic curve with the anodic curve facilitated with the corrosion potential by solving equation (45).

$$i_{Fe/Fe^{2+}} = i_{H_3O^+/H_2} + i_{HCO_3^-/CO_3^{2-}} + i_{H_2O/OH^-} + i_{PZH^+/PZ} + i_{MDEAH^+/MDEA} \quad (45)$$

Corrosion current is calculated from the anodic curve equation (28) at the known corrosion potential. Tafel extrapolation method was applied to determine the corrosion current density, which was used to calculate the corrosion rate by as in equation (46):

$$CR = \frac{i_{corr} M_w}{\rho\, nF} \chi = 1.155\, i_{corr} \quad (46)$$

Where, CR is the corrosion rate in mm/yr; i_{corr} is the corrosion current density in A/m^2; M_w is the molecular weight of iron in kg/mol.; ρ is the density of metal in kg/m^3; n is the number of electron exchanged in the electrochemical reaction, and χ is a unit conversion factor.

5. RESULTS AND DISCUSSION

5.1 Speciation of carbonated MDEA-PZ system

The calculated CO_2 loading of MDEA-PZ solution at different solution temperatures and CO_2 partial pressure is compared with experimental data from literature [5, 7] as shown in Figure 2. Similarly, the comparison of the calculated pH of solution at different CO_2 partial pressures is compared with experimental results [7] as shown in the Figure 3. Derk et al. [7] measured the pH of the aqueous MDEA+PZ solutions as a function of carbon dioxide loading, and their results are

compared with the model prediction as shown in Figure 3. From this Figure, it can be concluded that the model is able to predict the trend in pH fairly well, despite a seemingly constant offset between experimental values and model prediction. However, there seem to be a (consistent) discrepancy between the predicted and measured pH. This might be due to the interaction parameters used in the e-NRTL model to describe the molecular-molecular, molecular- ions, and ions-ions interaction in the solution which were taken from the work of Austgen et al. [17] as a defaults parameters. Both figures depicted a good agreement in the predicted and experimental results.

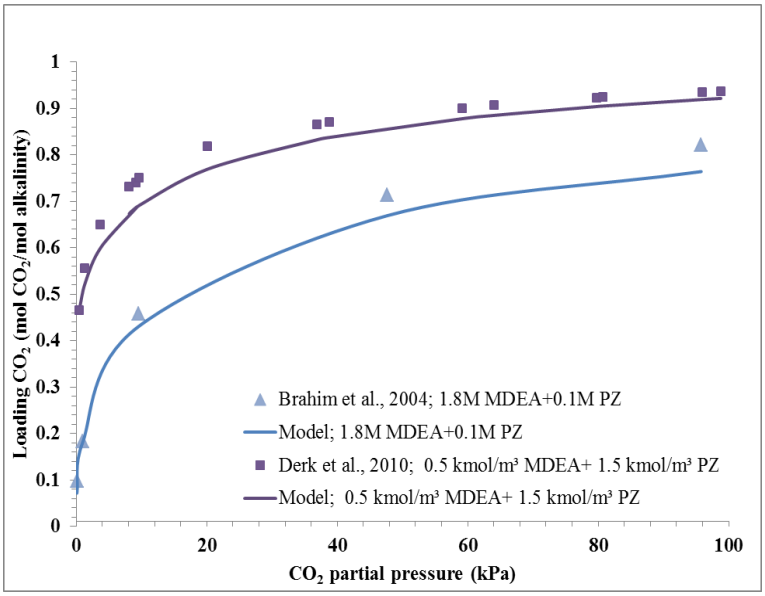

Figure 2. Comparison between calculated and experimental results of MDEA-PZ at 313.15 K

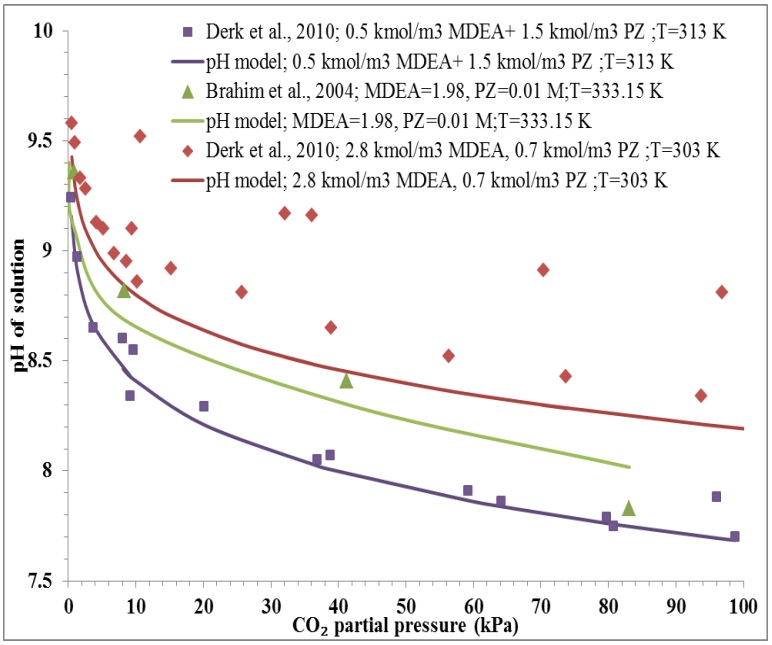

Figure 3. Assessment of experimental and calculated results of pH MDEA-PZ system.

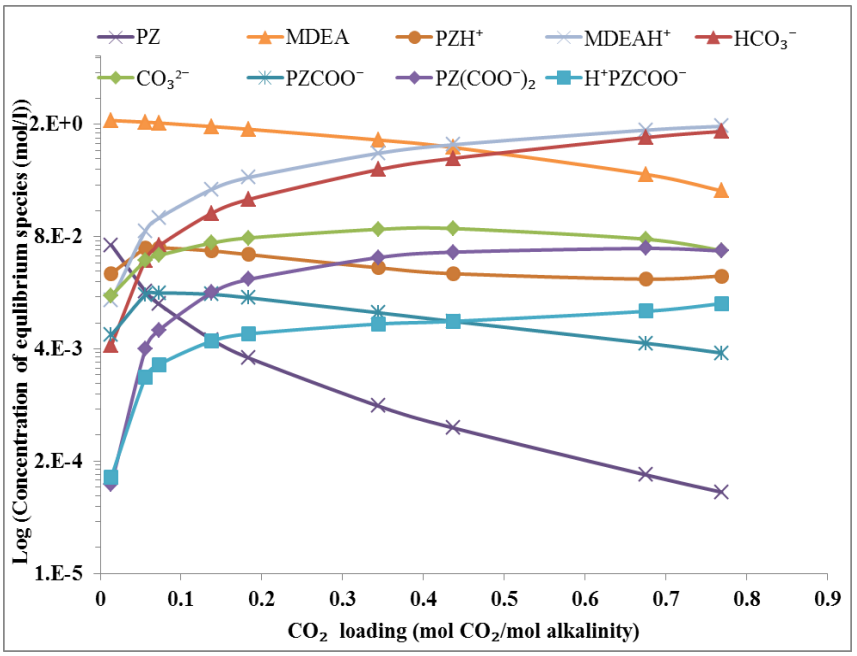

Figure 4. Predicted concentration of species in 1.8 M MDEA+ 0.1 M PZ system at 313.15 K

Due to the low concentration of piperazine in MDEA; the PZ species concentrations are low compared to that of MDEA species. Figure 4 represents the predicted species concentration, for the carbonated aqueous solution of 1.8M MDEA+0.1M PZ. It can be observed that a sharp decrease in PZ concentration at low CO_2 loading. This is due to the PZ reaction with CO_2, which is much faster than that of MDEA reaction with CO_2. Furthermore PZ forms carbamates and MDEA does not. Protonated piperazine and piperazine carbamate show a sudden increase till CO_2 loading point of 0.07 (mol CO_2/mol alkalinity), where both species reach to a maximum concentration at this CO_2 loading. The piperazine carbamates further react with CO_2 to give piperazine di-carbamate which appears at CO_2 loading of 0.14 (mol CO_2/mol alkalinity). It reached its maximum concentration at CO_2 loading of 0.6 (mol CO_2/mol alkalinity).

The increase in concentration of the piperazine di-carbamate and that of protonated piperazine carbamate lead to a decrease in the concentration of the protonated piperazine and piperazine carbamate. The behavior of MDEA species in the MDEA-PZ system is similar to that of aqueous carbonated MDEA. MDEA which does not form carbamates reacts with CO_2 only through an acid-base buffer mechanism in which CO_2 is converted primarily to bicarbonate. However, CO_2 must first react with H_2O to produce carbonic acid H_2CO_3, which subsequently dissociate to bicarbonate HCO_3^-, or it must react directly with OH^- to form bicarbonate. It is observed that the concentration of protonated MDEA and bicarbonate do not remain relatively similar through over all CO_2 loading range. The second dissociation constant of CO_2 is not negligible relative to its first dissociation constant, therefore a significant amount of carbonate is formed relative to bicarbonate. Hence, the concentration of bicarbonate is not in general equal to the concentration of protonated MDEA. Figure 4 also shows that at low CO_2 loading the concentration of $MDEAH^+$, HCO_3^-, PZH^+, and $PZCOO^-$

increased with increasing CO_2 loading but at high CO_2 loading the dominate species are $MDEAH^+$,HCO_3^-, PZH^+, $PZ(COO^-)_2$ and H^+PZCOO^-.

5.2 Carbon steel Corrosion rate in carbonated MDEA-PZ system

The developed corrosion rate model was used to simulate the corrosion process and to predict corrosion rate of carbon steel in aqueous MDEA-PZ systems. The simulation results were compared with experimental corrosion rate data. All comparisons were made using polarization curves and electrode kinetic data, including corrosion current density (i_{corr}), corrosion potential (E_{corr}), and corrosion rate, as shown in Figures 5-8 and Tables 8-11.

Figures 5 and 8 depict that the predicted and experimental polarization curves which are in good agreement. Polarization curves shift in the direction of lower corrosion current density which implies that the predicted corrosion rate values are lower than that obtained from experiments. The deviation of the simulated polarization curves might be due to the value of exchange current density of oxidizing agents which were assumed similar to those of aqueous MDEA system, as reported by Choi et al. [14].

Figures 5-8 and Tables 8-11 also show that the polarization curves produced from the model are closer to the experimental curves. It is evident that the corrosion potential from the model shifted toward lower values compared to the experimental data. The lower corrosion potential predicted from the model resulted from the mixed potential theory used in the model. As mentioned previously, the mixed potential theory is used to calculate the corrosion potential based on the summation of all partial reduction current equal to the oxidation currents.

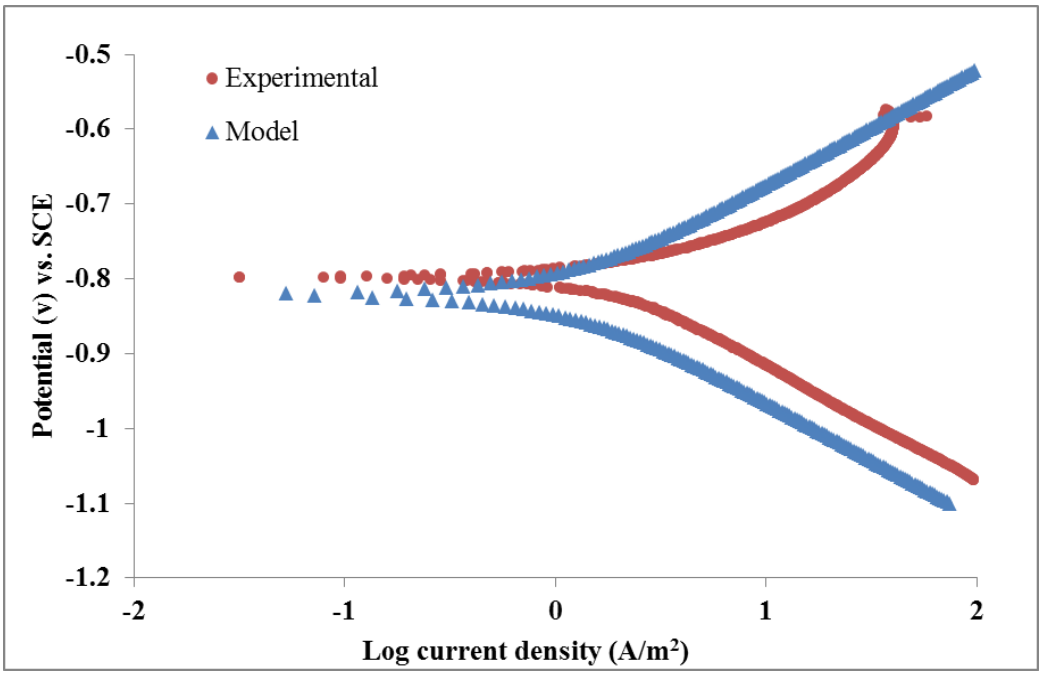

Figure 5. Comparison of predicted and experimental polarization curves of carbon steel in 1.98 M MDEA+0.01 M PZ; P_{CO2}= 47.55 kPa at 313.15 K

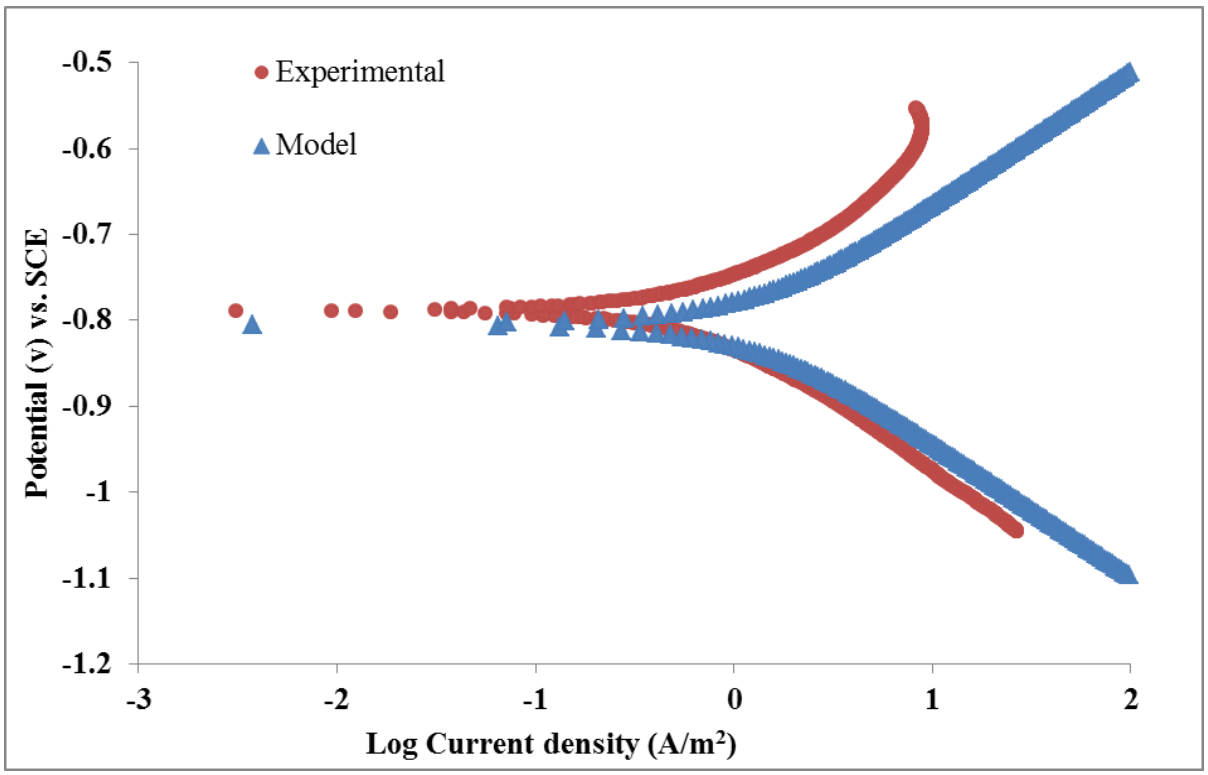

Figure 6. Comparison of predicted and experimental polarization curves of carbon steel in 1.9 M MDEA+ 0.05M PZ; P_{CO2}=95.27 kPa at 313.15 K

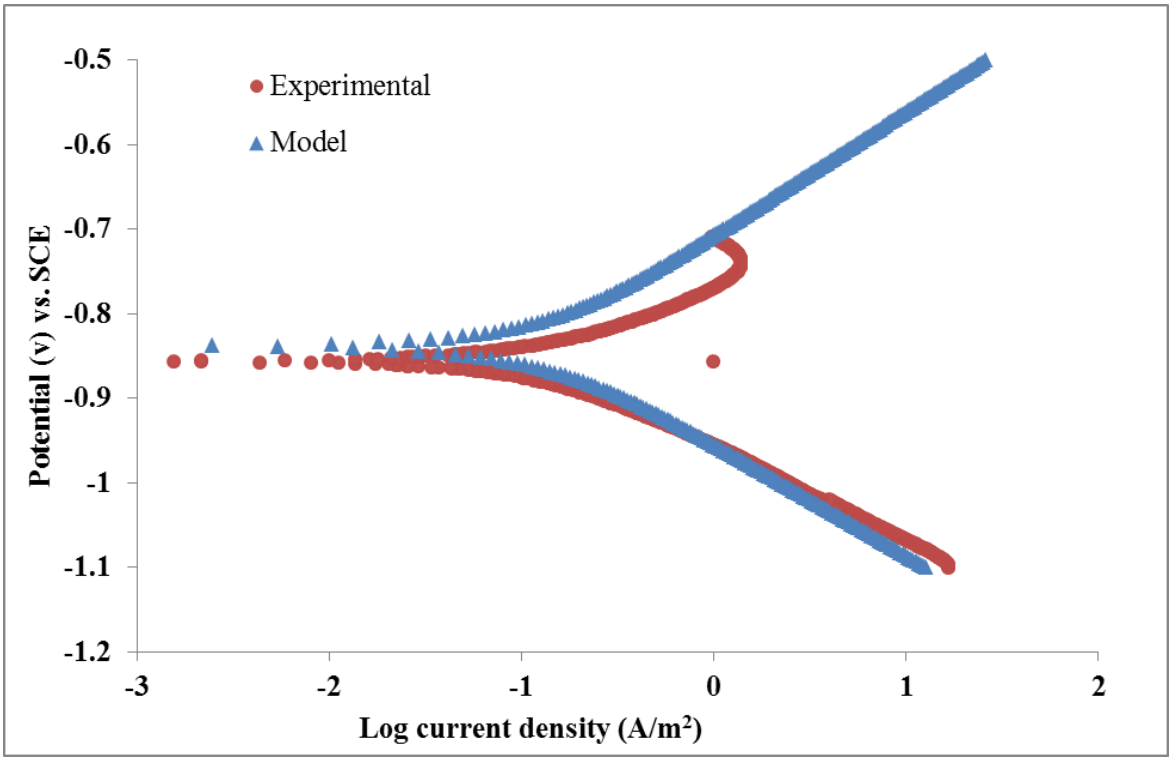

Figure 7. Comparison of predicted and experimental polarization curves of carbon steel in 1.98 M MDEA+0.01 M PZ; P_{CO2}= 0.83 kPa at 333.15 K

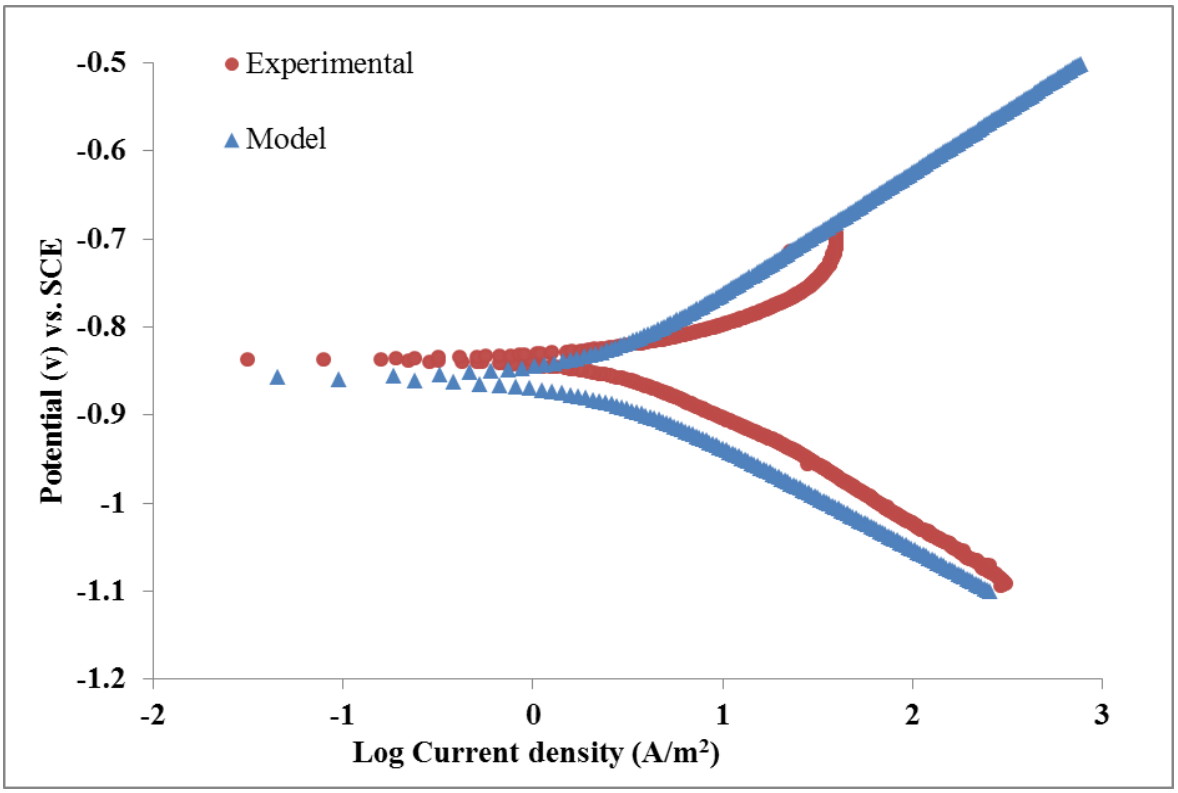

Figure 8. Comparison of predicted and experimental polarization curves of carbon steel in 1.8 M MDEA+ 0.1 M PZ; P_{CO_2}=55.47 kPa at 353.15 K

Table 8. Comparison of experimental and calculated of carbon steel corrosion data in aqueous 2 M MDEA solution

T(K)	P_{CO_2} (kPa)	Experimental		Model		δ^a	δ^b
		E_{corr} (Vvs.SCE)	CR (mm/yr)	E_{corr} (Vvs.SCE)	CR (mm/yr)		
313.15	0.96	-0.84	0.22	-0.82	0.18	2.41	19.51
	9.56	-0.80	0.84	-0.83	0.78	3.21	7.63
	47.72	-0.80	1.31	-0.82	1.49	2.64	14.07
	95.61	-0.79	1.76	-0.80	1.72	1.76	2.23
333.15	0.83	-0.86	0.46	-0.84	0.15	2.12	66.57
	8.31	-0.82	1.15	-0.85	0.81	3.16	30.11
	41.45	-0.82	1.75	-0.84	2.09	2.62	19.63
	82.91	-0.82	2.23	-0.84	2.82	2.61	26.29
353.15	0.55	-0.86	0.10	-0.84	0.11	2.53	9.19
	5.55	-0.86	1.19	-0.86	0.61	0.19	48.58
	27.57	-0.84	1.47	-0.87	1.83	2.89	24.15
	55.48	-0.85	2.92	-0.86	2.83	2.14	3.10

$$\delta^a = \frac{\left|E_{corr(Cal.)} - E_{corr(Exp.)}\right|}{E_{corr(Exp.)}} \times 100 \,, \delta_{AAD} = 2.36\%$$

$$\delta^b = \frac{\left|\mathrm{CR}_{(Cal.)} - \mathrm{CR}_{(Exp.)}\right|}{\mathrm{CR}_{(Exp.)}} \times 100 \,, \delta_{AAD} = 22.59\%$$

Table 9. Comparison of experimental and calculated of carbon steel corrosion data in aqueous 1.98 M MDEA +0.01 M PZ solution

T(K)	P_{CO_2} (kPa)	Experimental		Model		δ^a	δ^b
		E_{corr} (V)	CR (mmpy)	E_{corr} (V)	CR (mmpy)		
313.15	0.95	-0.85	0.25	-0.82	0.17	3.28	34.73
	9.54	-0.80	0.60	-0.83	0.69	4.04	15.37
	47.55	-0.80	1.28	-0.82	1.36	2.82	6.23
	95.28	-0.79	1.65	-0.81	1.60	2.73	2.98
333.15	0.83	-0.86	0.37	-0.84	0.15	2.19	58.28
	8.26	-0.83	0.73	-0.85	0.74	2.52	2.00
	41.20	-0.83	1.63	-0.85	1.85	2.06	13.75
	83.07	-0.82	2.02	-0.84	2.52	2.94	24.73
353.15	0.56	-0.86	0.31	-0.84	0.12	2.46	61.45
	5.55	-0.86	0.95	-0.86	0.60	0.06	37.24
	27.57	-0.82	1.66	-0.86	1.70	4.83	2.24
	55.31	-0.84	2.35	-0.86	2.56	2.32	8.79

$$\delta^a = \frac{\left|E_{corr(Cal.)} - E_{corr(Exp.)}\right|}{E_{corr(Exp.)}} \times 100 \,, \delta_{AAD} = 2.69\%$$

$$\delta^b = \frac{\left|\mathrm{CR}_{(Cal.)} - \mathrm{CR}_{(Exp.)}\right|}{\mathrm{CR}_{(Exp.)}} \times 100 \,, \delta_{AAD} = 22.32\%$$

Table 10. Comparison of experimental and calculated of carbon steel corrosion data in aqueous 1.9 M MDEA +0.05 M PZ solution

T(K)	P_{CO_2} (kPa)	Experimental		Model		δ^a	δ^b
		E_{corr} (V)	CR (mmpy)	E_{corr} (V)	CR (mmpy)		
313.15	0.95	-0.84	0.28	-0.82	0.16	2.62	41.49
	9.58	-0.81	0.49	-0.83	0.65	1.28	33.55
	47.55	-0.79	1.44	-0.82	1.26	3.42	12.57
	95.78	-0.79	1.32	-0.80	1.48	1.89	12.75
333.15	0.83	-0.85	0.26	-0.84	0.17	1.98	34.45
	8.29	-0.84	0.63	-0.85	0.74	0.57	18.56
	41.28	-0.81	1.69	-0.84	1.79	4.50	6.18
	83.24	-0.82	1.70	-0.84	2.41	1.94	41.86
353.15	0.55	-0.83	0.18	-0.85	0.14	1.57	23.97
	5.55	-0.83	0.89	-0.86	0.64	3.70	27.78
	27.49	-0.83	1.56	-0.86	1.72	4.37	10.69
	55.64	-0.84	2.02	-0.86	2.57	2.21	27.07

$$\delta^a = \frac{\left|E_{corr(Cal.)} - E_{corr(Exp.)}\right|}{E_{corr(Exp.)}} \times 100 \,, \delta_{AAD} = 2.50\%$$

$$\delta^b = \frac{\left|\mathrm{CR}_{(Cal.)} - \mathrm{CR}_{(Exp.)}\right|}{\mathrm{CR}_{(Exp.)}} \times 100 \,, \delta_{AAD} = 24.24\%$$

Table 11. Comparison of experimental and calculated of carbon steel corrosion data in aqueous 1.8 M MDEA +0.1 M PZ solution

T(K)	P_{CO2} (kPa)	Experimental		Model		δ^a	δ^b
		E_{corr} (V)	CR (mmpy)	E_{corr} (V)	CR (mmpy)		
313.15	0.95	-0.79	0.21	-0.81	0.16	3.28	23.13
	9.59	-0.79	0.44	-0.82	0.61	3.43	38.76
	47.64	-0.78	1.46	-0.81	1.15	3.14	20.93
	95.78	-0.79	1.17	-0.80	1.35	1.18	15.52
333.15	0.83	-0.87	0.27	-0.83	0.18	4.00	33.02
	8.31	-0.83	0.50	-0.84	0.75	0.96	48.27
	41.45	-0.83	1.71	-0.84	1.72	1.17	1.13
	83.41	-0.82	1.24	-0.83	2.29	1.22	85.46
353.15	0.55	-0.86	0.17	-0.85	0.16	1.05	5.07
	5.58	-0.83	0.81	-0.86	0.69	3.08	14.78
	27.74	-0.84	1.48	-0.86	1.77	2.29	19.00
	55.48	-0.84	1.83	-0.86	2.56	2.27	39.85

$$\delta^a = \frac{\left|E_{corr(Cal.)} - E_{corr(Exp.)}\right|}{E_{corr(Exp.)}} \times 100 \,, \delta_{AAD} = 2.26\%$$

$$\delta^b = \frac{\left|\mathrm{CR}_{(Cal.)} - \mathrm{CR}_{(Exp.)}\right|}{\mathrm{CR}_{(Exp.)}} \times 100 \,, \delta_{AAD} = 28.75\%$$

5.3 Effect of CO_2 loading and PZ concentration on Corrosion rate

The effect of CO_2 loading is demonstrated by comparing the model with experimental results in aqueous MDEA-PZ solutions. Figures 9 and Figure 10 illustrate that the CO_2 loading has a significant effect on corrosion rate of carbon steel. At high CO_2 loading the solution is more corrosive than that at low CO_2 loading. For instance, the carbon steel corrosion rate in 2M MDEA system increased from 0.22 to 1.76 mm/yr as the CO_2 loading increased from 0.15 to 0.88 (mol of CO_2/ mol alkalinity) at 40 °C. Such increase in corrosion rate is due to the increase in dissolved CO_2 to form HCO_3^- and $MDEAH^+$, which induces more iron dissolution. This is evidenced by greater cathodic current densities in Figure 9. Similar results with respect to HCO_3^- concentration effect on carbon steel corrosion rate has investigated by Choi et al. [14] in their work on carbonated aqueous MDEA system's corrosivity. They concluded that corrosion rate of carbon steel increased with increasing in HCO_3^- concentration with a reaction order 2 for iron dissolution reaction under different test conditions. Furthermore, Duan

et al. [34] evaluated the corrosion properties of carbon steel in 50 wt% MDEA systems at 50 °C with different CO_2 partial pressures. They found under the absorber conditions, the addition of CO_2 in MDEA systems significantly increased the corrosion rate and changed behavior from a passive to an active state. They also concluded that the dominant cathodic reactions in aqueous carbonated MDEA system are HCO_3^- and $MDEAH^+$ reduction reactions.

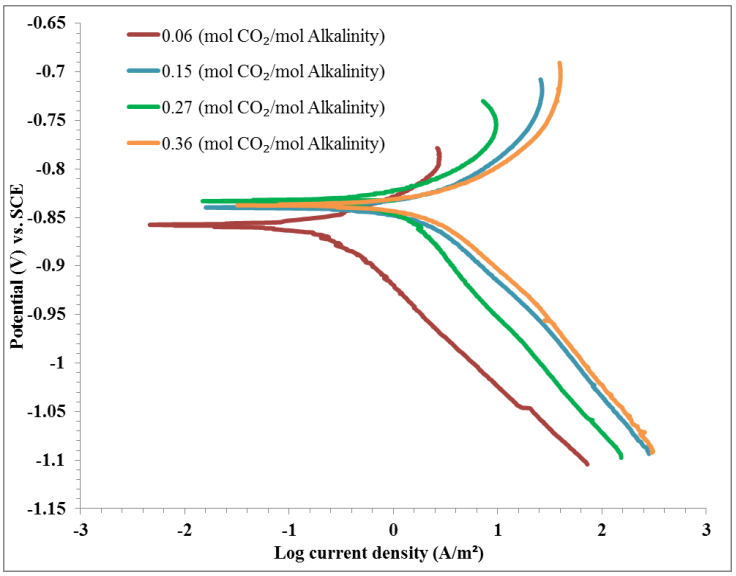

Figure 9. Effect of CO_2 loading on polarization behavior of carbon steel in MDEA-PZ solution with a concentration 1.8M MDEA+0.1M PZ at 80 °C

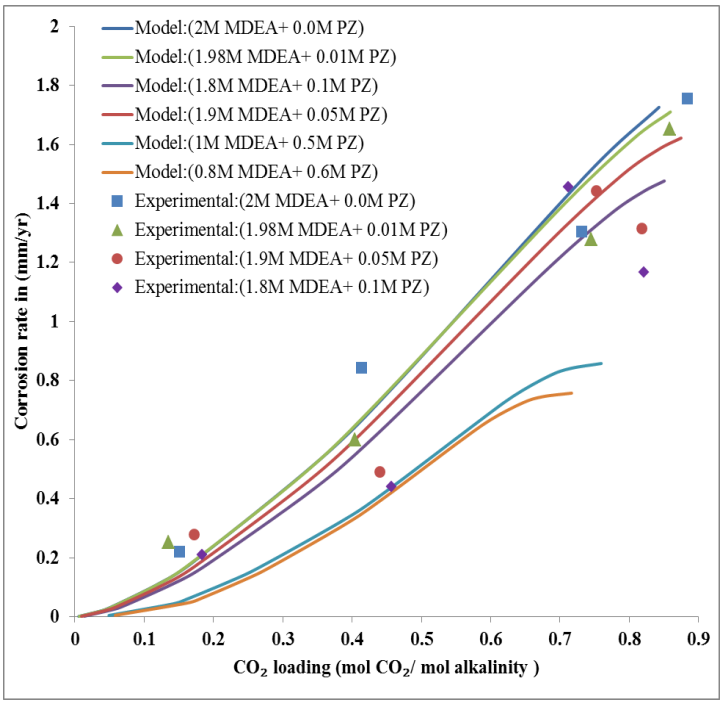

Figure 10. Effect of CO_2 loading on carbon steel corrosion rate in MDEA-PZ aqueous solution at T=313.15 K

However, in MDEA-PZ systems and for a constant total amine concentration with increasing the concentration of PZ appears to nullify the rate as noticed in Figure 10. The effect of PZ concentration on corrosion rate was found to be dependent on the CO_2 loading. As shown in Figure 11, at low CO_2 loading (low CO_2 partial pressure) concentrations of the oxidizing species are very low therefore the effect of temperature is more than the effect of addition of piperazine even it is working as an activator to MDEA to increase the CO_2 loading in the solution and increasing corrosion rate. However, at high CO_2 loading (high CO_2 partial pressure) the addition of piperazine to the MDEA solution will_decrease the system ability to absorb CO_2 which means a decrease in oxidizing agent concentration in the solution thereby decreases corrosion rate. This is believed to be due to the concentration of HCO_3^- in the systems, at low CO_2 partial pressure the increase in PZ concentration yields higher amount of HCO_3^-, which in turn dissociate and due to the increasing in CO_2 loading, the increasing in CO_2 loading drives the corrosion process to proceed faster, thus causing increasing in corrosion rate while at high CO_2 partial pressure, the addition of PZ concentration leads to decrease in HCO_3^- concentration which in turn decreasing in CO_2 loading and leads to decrease in corrosion rate.

The high corrosion rate in 2 M MDEA, compared to that of MDEA-PZ under the same conditions of (CO_2 loading, solution temperature and PZ concentration) is due to high bicarbonate concentration.

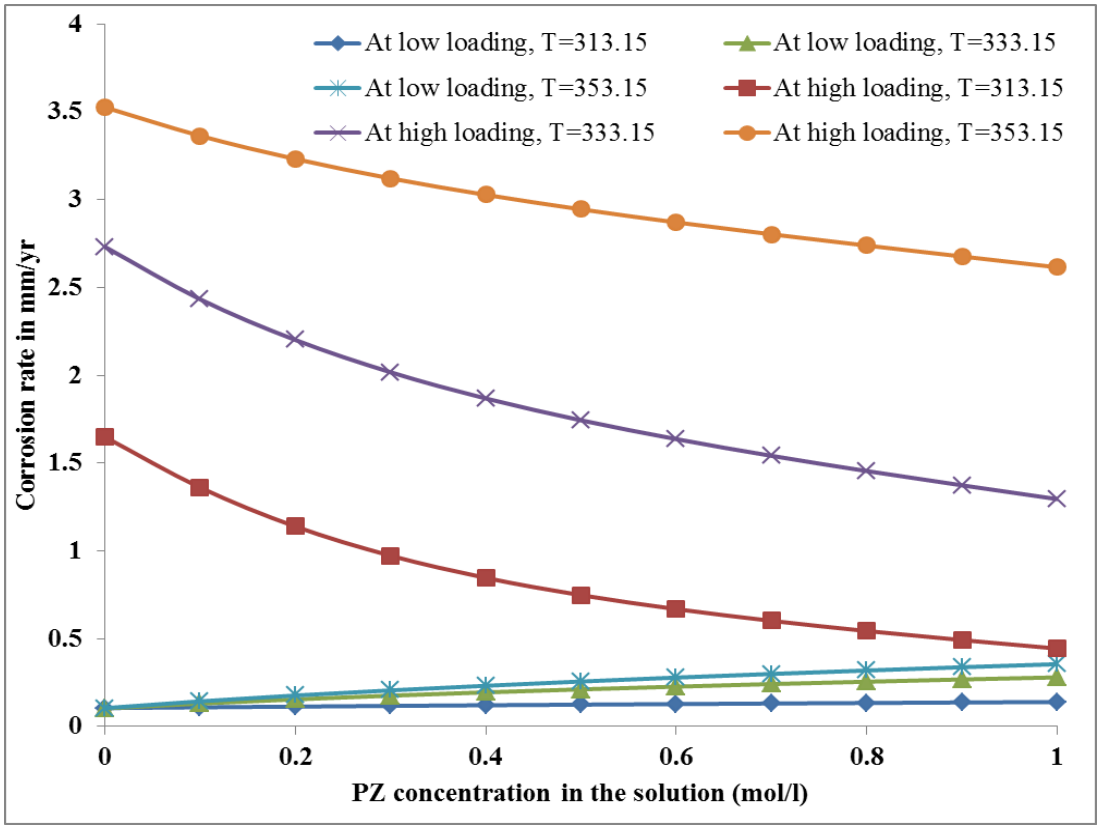

Figure 11. Effect of PZ concentration on the carbon steel corrosion rate in MDEA-PZ aqueous solution at three solution temperature

5.4 Effect of temperature on corrosion rate

The effect of solution temperature on corrosion rate was investigated at different CO_2 loadings. The increase of solution temperature will result in a decrease of the CO_2 loading in aqueous MDEA-PZ systems and thereby decrease the concentration of oxidizing agent in the solution, in which the corrosion process depends on the flow of oxidizing agent at the carbon steel surface. The corrosion results as shown in Figures 12 and 13 show that the solution temperature has a considerable effect on corrosion rate, an increase in solution temperature lead to an increase in corrosion rate. This can be explained by the dependence of reaction kinetics on temperature. It is well established that the reaction rate increases with temperature according to Arrhenius theory. Therefore, the increase in temperature increases rates of metal dissolution and oxidizer reduction, thereby accelerating the corrosion rate.

In the absence of any precipitation and corrosion product layer formation in the carbonated activated MDEA system, temperature accelerates the kinetics of all the process involved in a corroding system: electrochemical reactions, chemical reactions, and transport processes. Hence the final corrosion rate also increases with temperature as indicated in Figures 12 and 13, as is expected. The corrosion rate, which is under charge transfer at initial temperature, become mass transfer limiting current controlled at higher temperatures. The temperature dependence of the carbonated aqueous solutions of MDEA-PZ viscosity at a given CO_2 loading and a given concentration of PZ and MDEA, exponentially decreases with increasing temperature. The effect of decreasing viscosity with increases in temperature for aqueous carbonated MDEA-PZ solution can be found in the work by [33]. The increasing in solution temperature led to decrease the viscosity of solution with increase in corrosive species diffusivity according to the Stockes-Einstein equation, decreased pathways for corrosive species to reach the surface of carbon steel, which leads to high carbon steel dissolution.

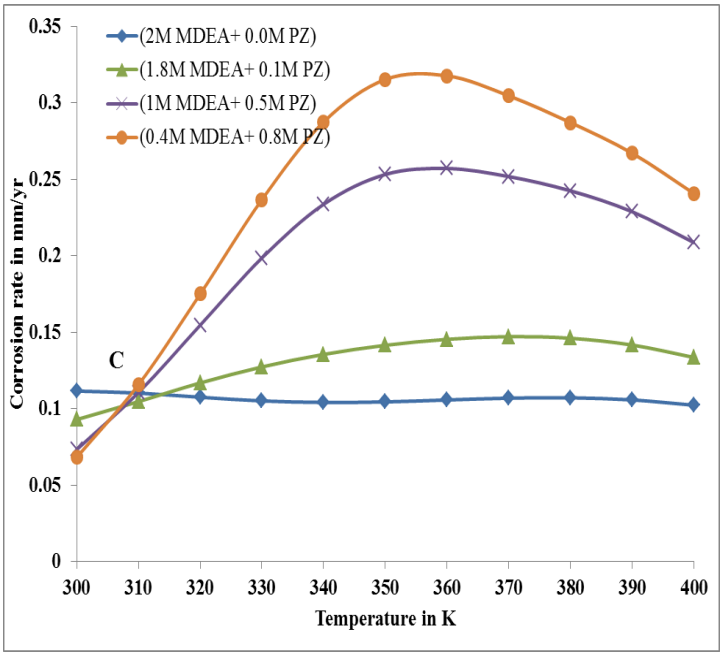

Figure 12. Effect of temperature on carbon steel corrosion rate in aqueous MDEA-PZ solutions at low CO_2 loading

On the other hand, the corrosion rate decreases with the increase in the PZ concentration with a crossover point (indicated by point C) as shown in Figures 12 and 13. Moreover, by increasing temperature the crossover point shifts toward a higher corrosion rate.

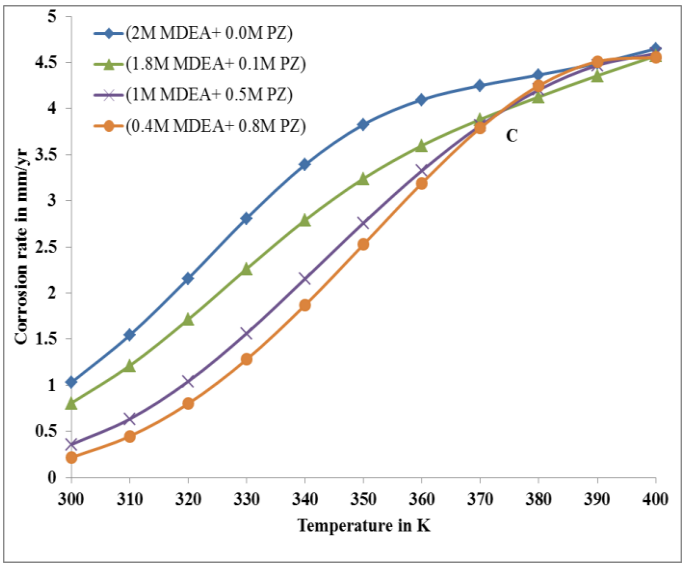

Figure 13. Effect of temperature on corrosion of carbon steel in the MDEA-PZ solutions at high CO_2 loading

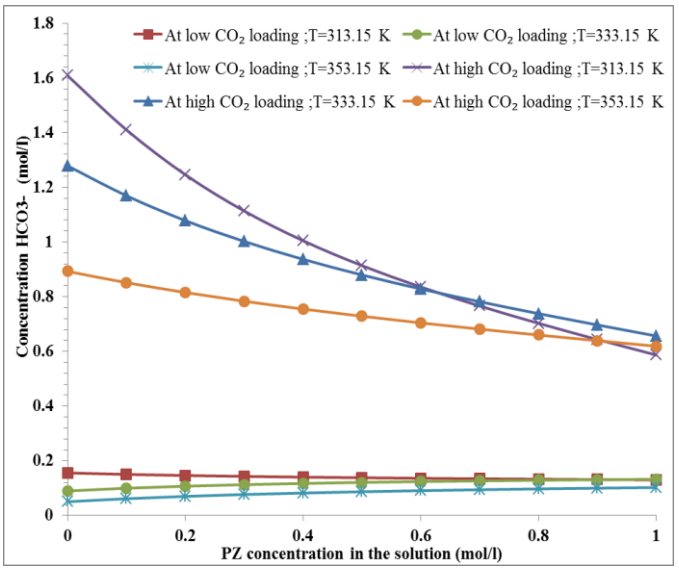

Figure 14. Effect of HCO_3^- concentration on the carbon steel corrosion rate in aqueous MDEA-PZ solution at three solution temperatures

This crossover point might be because of addition of PZ concentration in the solution. At low CO_2 partial pressure, the addition of PZ concentration to the aqueous MDEA solution increased the CO_2 loading when compared MDEA alone. The addition of PZ to MDEA increases the bicarbonate and protonated amine concentrations which are the main oxidizing agents affecting the corrosion process of carbon steel which led to increase the corrosion rate, whereas at high CO_2 partial pressure

the corrosion rate of carbon steel decreased in the MDEA-PZ system, this is because of the decreasing in the HCO_3^- concentration which is the main oxidizing agents affecting the corrosion process of carbon steel as shown in figure 14. The effect of PZ concentration on CO_2 loading in the aqueous carbonated MDEA-PZ solution at high and low CO_2 partial pressure can be found in the work by [5].

5.5 Effect of corrosion potential

Figure 15 shows the change of corrosion potential for carbon steel in the carbonated PZ-MDEA system at different PZ concentrations. At low partial pressure of CO_2 (< 1 kPa), carbon steel shows active behavior with potential -0.84 V vs SCE and increases to -0.79 V vs SCE at high CO_2 partial pressure in 2 M MDEA solution at 313.15 K. However, there is an increase in potential with increase in PZ concentration indicating the corrosion behavior changes from active to the passive by increasing CO_2 partial pressure. This can be explained by a decrease in HCO_3^- and $MDEAH^+$ concentration in the MDEA-PZ systems at high CO_2 partial pressure and PZ concentration, which they are main oxidizing agents, lead to corrode the carbon steel surface.

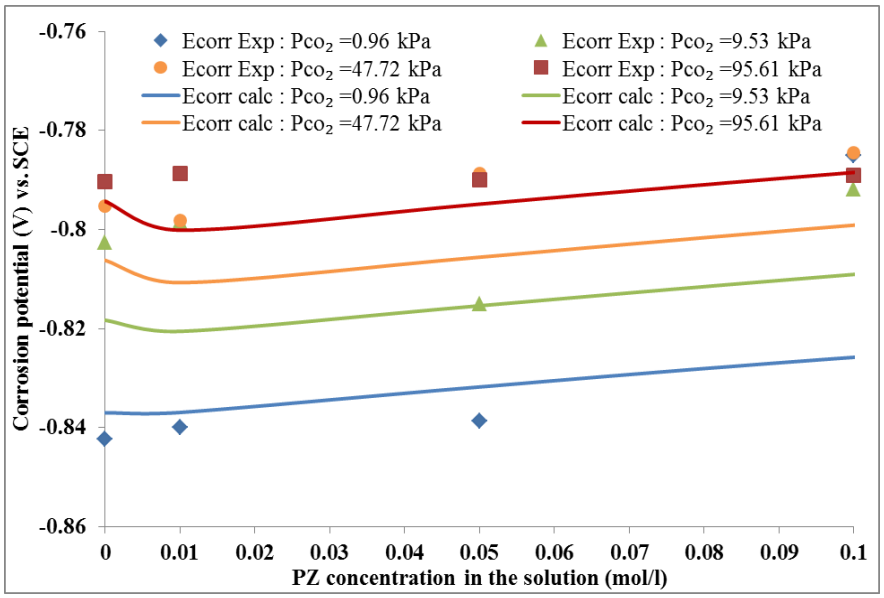

Figure 15. Variation in corrosion potential for carbon steel as a function of PZ concentration in carbonated MDEA-PZ system at low CO_2 partial pressure, 313.15 K

6. CONCLUSIONS

A comprehensive model was developed for simulating the polarization curves of carbon steel in aqueous carbonated MDEA-PZ systems. The model consists of a thermodynamic model that provides speciation calculations and an electrochemical model that predicts the partial reduction and oxidation processes on the surface of the metal. The model has been validated extensively using thermodynamic and corrosion rate experimental data. Good agreement with experimental results was obtained for most

of the cases. The model adequately represents the effect of PZ concentration, solution temperature and CO_2 loading on the carbon steel corrosion rate in aqueous carbonated solutions of MDEA-PZ. The corrosivity of carbon steel in aqueous carbonated solution of MDEA-PZ was governed mainly by their CO_2 loading such that higher CO_2 loading led to higher corrosion rate. At low CO_2 loading the corrosion rate of carbon steel increased with increasing in solution temperature and PZ concentration whereas, at high CO_2 loading the corrosion rate decreased with increasing solution temperature and PZ concentration.

This model is also used to identify the oxidizing agents responsible for corrosion of carbon steel in aqueous carbonated activated MDEA systems. HCO_3^- contributes the most to the changes in corrosion kinetics at higher temperatures and higher CO_2 loading, while H_3O^+ and H_2O contribute the least at high pH condition. The protonated MDEA and protonated PZ contribute as oxidizing agents based on the concentration of that amine in the solution. Developed models and results of the current study may serve as a prediction tool for designing CO_2 absorption systems at conditions that have not been investigated experimentally.

ACKNOWLEDGEMENTS
This research is supported by High Impact Research Grant UM.C/625/1/HIR/123, from University of Malaya, Kuala Lumpur 50603, Malaysia

References

1. B. S. Ali, B. Ali, R. Yusoff and M. Aroua, *International Journal of Electrochemical Science*, 7 (2012) 3835.
2. S. A. Mazari, B. S. Ali, B. M. Jan, I. M. Saeed and S. Nizamuddin, *International Journal of Greenhouse Gas Control*, 34 (2015) 129.
3. P. Gunasekaran, A. Veawab and A. Aroonwilas, *Energy Procedia*, 37 (2013) 2094.
4. A. Kunjunny, M. Patel and N. Nath, *Fertiliser news*, 44 (1999) 53.
5. B. S. Ali and M. Aroua, *International journal of thermophysics*, 25 (2004) 1863.
6. S. Bishnoi and G. T. Rochelle, *AIChE Journal*, 48 (2002) 2788.
7. P. Derks, J. Hogendoorn and G. Versteeg, *The Journal of Chemical Thermodynamics*, 42 (2010) 151.
8. H. Dang and G. T. Rochelle, *Separation science and technology*, 38 (2003) 337.
9. J. T. Cullinane and G. T. Rochelle, *Chemical Engineering Science*, 59 (2004) 3619.
10. B. Zhao, Y. Sun, Y. Yuan, J. Gao, S. Wang, Y. Zhuo and C. Chen, *Energy Procedia*, 4 (2011) 93.
11. M. Nainar and A. Veawab, *Industrial & Engineering Chemistry Research*, 48 (2009) 9299.
12. X.-P. Guo and Y. Tomoe, *Corrosion science*, 41 (1999) 1391.
13. L. Zheng, J. Landon, W. Zou and K. Liu, *Industrial & Engineering Chemistry Research*, 53 (2014) 11740.
14. Y.-S. Choi, S. Nešić, D. Duan and S. Jiang, in *CORROSION 2012* (2012).
15. B. S. Ali, PhD Thesis. University of Malaya (2007).
16. S. Bishnoi and G. T. Rochelle, *Industrial & engineering chemistry research*, 41 (2002) 604.
17. D. M. Austgen, G. T. Rochelle, X. Peng and C. C. Chen, *Industrial & Engineering Chemistry Research*, 28 (1989) 1060.
18. B. E. Poling, J. M. Prausnitz and J. P. O'connell, The properties of gases and liquids, McGraw-Hill New York (2001).

19. G. Soave, *Chemical Engineering Science*, 27 (1972) 1197.
20. M. L. Posey and G. T. Rochelle, *Industrial & engineering chemistry research*, 36 (1997) 3944.
21. S. Moioli and L. A. Pellegrini, *Chemical Engineering Research and Design*, 93 (2015) 611.
22. S. K. Dash, A. Samanta, A. N. Samanta and S. S. Bandyopadhyay, *Fluid Phase Equilibria*, 300 (2011) 145.
23. A. Veawab, PhD Thesis. University of Regina (2001).
24. N. Sadegh, *Technical University of Denmark, DK-2800 Lyngby, Denmark* (2012).
25. R. N. Goldberg, N. Kishore and R. M. Lennen, *Journal of physical and chemical reference data*, 31 (2002) 231.
26. S. Nesic, J. Postlethwaite and S. Olsen, *Corrosion*, 52 (1996) 280.
27. M. Eisenberg, C. Tobias and C. Wilke, *Journal of the Electrochemical Society*, 101 (1954) 306.
28. R. H. Weiland, J. C. Dingman, D. B. Cronin and G. J. Browning, *Journal of Chemical & Engineering Data*, 43 (1998) 378.
29. P. Atkins, J. De Paula and R. Friedman, Physical Chemistry: Quanta, Matter, and Change, Oxford University Press (2013).
30. S. Nesic, R. Nyborg, A. Stangeland and M. Nordsveen, in *CORROSION 2001* (2001).
31. R. L. Rowley, M. E. Adams, T. L. Marshall, J. L. Oscarson, W. V. Wilding and D. J. Anderson, *Journal of Chemical & Engineering Data*, 42 (1997) 310.
32. P. W. Derks, E. S. Hamborg, J. Hogendoorn, J. P. Niederer and G. F. Versteeg, *Journal of Chemical & Engineering Data*, 53 (2008) 1179.
33. D. Fu, L. Qin and H. Hao, *Journal of Molecular Liquids*, 186 (2013) 81.
34. D. Duan, Y.-S. Choi, S. Jiang and S. Nešic, *CORROSION/2013, paper* (2013).